Hybrid core-shell particles for mRNA systemic delivery

Valentina Andretto, Mathieu Repellin, Marine Pujol, Eyad Almouazen, Jacqueline Sidi-Boumedine, Thierry Granjon, Heyang Zhang, Katrien Remaut, Lars Petter Jordheim, Stéphanie Briançon, et al.

Journal of Controlled Release 353 (2023) 1037–1049

Contents lists available at ScienceDirect

Journal of Controlled Release

journal homepage: www.elsevier.com/locate/jconrel

Hybrid core-shell particles for mRNA systemic delivery

Valentina Andretto [a], Mathieu Repellin [a], Marine Pujol [a], Eyad Almouazen [a], Jacqueline Sidi-Boumedine [a], Thierry Granjon [b], Heyang Zhang [c], Katrien Remaut [c], Lars Petter Jordheim [d], Stéphanie Briançon [a], Isabel Sofia Keil [e], Fulvia Vascotto [e], Kerstin C. Walzer [f], Ugur Sahin [f], Heinrich Haas [f], David Kryza [a,g], Giovanna Lollo [a,*]

[a] Univ. Lyon, Université Claude Bernard Lyon 1, CNRS, LAGEPP UMR 5007, 43 Boulevard du 11 Novembre 1918, F-69622, Villeurbanne, France
[b] Institut de Chimie et Biochimie Moléculaires et Supramoléculaires, ICBMS UMR 5246, Université de Lyon, Université Lyon 1, CNRS, F-69622 Lyon, France
[c] Ghent Research Group on Nanomedicine, Laboratory of General Biochemistry and Physical Pharmacy, Faculty of Pharmaceutical Sciences, Ghent University, 9000 Ghent, Belgium
[d] Univ. Lyon, Université Claude Bernard Lyon 1, INSERM 1052, CNRS 5286, Centre Léon Bérard, Centre de Recherche en Cancérologie de Lyon, Lyon 69008, France
[e] TRON Translational Oncology at the University Medical Center of the Johannes Gutenberg University gGmbH, Mainz, Germany
[f] BioNTech SE, An der Goldgrube 12, 55131 Mainz, Germany
[g] Hospices Civils de Lyon, 69437 Lyon, France

ARTICLE INFO

Keywords:
Hybrid lipid-polymer nanoparticles
Core-shell nanoparticles
Lipoplexes
Hyaluronic acid
IVT mRNA
In vivo biodistribution

ABSTRACT

mRNA based infectious disease vaccines have opened the venue for development of novel nucleic acids-based therapeutics. For all mRNA therapeutics dedicated delivery systems are required, where different functionalities and targeting abilities need to be optimized for the respective applications. One option for advanced formulations with tailored properties are lipid-polymer hybrid nanoparticles with complex nanostructure, which allow to combine features of several already well described nucleic acid delivery systems. Here, we explored hyaluronic acid (HA) as coating of liposome-mRNA complexes (LRCs) to investigate effects of the coating on surface charge, physicochemical characteristics and biological activity. HA was electrostatically attached to positively charged complexes, forming hybrid LRCs (HLRCs). At different N/P ratios, physico-chemical characterization of the two sets of particles showed similarity in size (around 200 nm) and mRNA binding abilities, while the presence of the HA shell conferred a negative surface charge to otherwise positive complexes. High transfection efficiency of LRCs and HLRCs *in vitro* has been obtained in THP-1 and human monocytes derived from PBMC, an interesting target cell population for cancer and immune related pathologies. In mice, quantitative biodistribution of radiolabeled LRC and HLRC particles, coupled with bioluminescence studies to detect the protein translation sites, hinted towards both particles' accumulation in the hepatic reticuloendothelial system (RES). mRNA translated proteins though was found mainly in the spleen, a major source for immune cells, with preference for expression in macrophages. The results showed that surface modifications of liposome-mRNA complexes can be used to fine-tune nanoparticle physico-chemical characteristics. This provides a tool for assembly of stable and optimized nanoparticles, which are prerequisite for future therapeutic interventions using mRNA-based nanomedicines.

1. Introduction

The recent success of mRNA-based COVID-19 vaccines has impressively demonstrated the potential of nucleic acid-based therapeutics. However, in order to fully leverage the potential of mRNA there is still the need to improve selectivity and efficiency of mRNA-coded protein expression, in particular outside the field of prophylactic vaccination [1]. For example, for applications in which a higher amount of encoded protein is required or for systemic delivery, the availability of precise delivery systems is still an unmet demand. The use of *in vitro* transcribed (IVT) mRNA is currently widely explored for different therapeutic applications as gene editing, genetic reprogramming, cancer treatment, infectious diseases, vaccines, and many others. mRNA has several advantages in comparison to previously investigated DNA-based

* Corresponding author.
E-mail address: giovanna.lollo@univ-lyon1.fr (G. Lollo).

https://doi.org/10.1016/j.jconrel.2022.11.042
Received 19 July 2022; Received in revised form 15 November 2022; Accepted 22 November 2022
Available online 22 December 2022

therapeutics, as it does not integrate the genome eliminating the risk of carcinogenesis, and it does not require nuclear localization for protein expression [2]. However, delivery of cargo to site of translation is still a major challenge within the development of mRNA-based therapeutics. Over the past decades, both viral and non-viral vectors have been extensively studied for nucleic acids delivery [3]. Non-viral vectors offer several advantages compared to the viral ones, as reduced immunogenicity, and the possibility to deliver higher payloads, in addition to their easier manufacturing processes [4,5]. Various non-viral delivery systems, including polymer- [6], peptide- [7], and lipid-based [8] nanoparticles have been extensively studied. Among them, lipid nanoparticles (LNPs), have gained great public attention due to the recent approval of Onpattro® [9] and that of the two mRNA-based vaccines Cominarty [10] and Spikevax [11], all LNP-based RNA therapeutics.

In the present work, we focused on the design, physico-chemical characterization and *in vitro/in vivo* behavior of hybrid lipid nanosystems intended for the intra-venous administration of mRNA. Lipid-polymer hybrid systems allow the combination of the structural versatility features given by the lipid membranes, with the widely tunable properties of polymers. Depending on their characteristics, polymers can be combined with the lipid architecture in different ways, as simple coating to form a core-shell system, or by intercalation within the bilayer [8,12]. Here, we assembled hybrid nanoparticle formulations consisting of lipoplexes obtained from cationic liposomes and mRNA interaction, which were further functionalized with the anionic biopolymer hyaluronic acid (HA). Assembly of HA on top of lipoplexes may be considered an option to improve the formulation stability, to reduce aggregation and fast clearance followed by opsonization by serum proteins in circulation, which classically is obtained by PEG-conjugation [13]. PEGylation is a widely used strategy, but it is progressively considered critical since it can induce the production of anti-PEG antibodies, with consequent immune responses [14]. Nucleic acids delivery systems based on HA have been extensively studied over the years showing their potential applications in the field [15–17]. Previous studies already reported the use of other anionic polymers (such as alginates and polyglutamates) to increase the stability of lipid nanoparticles complexed with siRNA, and that of the nucleic acid itself, upon incubation in biological media [18]. Besides the physicochemical properties' improvement, HA can provide a targeting platform, as in the case of interaction/binding with CD44 receptors which is activating a number of pathways involved in cancer cell growth, survival, and metastasis [19]. Moreover, some groups present in HA structure such as hydroxyl, carboxyl, and *N*-acetyl are suitable for further chemical modification, making it an ideal candidate for a number of applications [20].

The liposome precursors for the nanoparticles prepared in this work were assembled from a mixture of the positively charged synthetic lipid DOTAP, the phospholipid DOPE as helper lipid, and ssPalm as pH-sensitive, cleavable lipid. DOTAP is among the most established cationic lipids for nucleotides delivery, for its sound ability to efficiently complex genetic material [21]. The zwitterionic DOPE is able to promote fusion with cells or endosomal membranes, favoring the intracellular release of the nucleic acids in the cytosol [22]. To facilitate the release of mRNA in the cytosol and enhance the endosomal escape, a disulfide bond (SS) cleavable pH-activated lipid-like material (ssPalm) has been added to the lipid mixtures [23]. The scaffold of ssPalm used in this study was myristic acid (ssPalmM), giving an innovative feature to the DOTAP/DOPE mixture, that has been recently patented for nucleic acid complexation [24]. The described cationic liposomes have been used for the formulation of mRNA to form lipoplexes. Here, we investigated lipoplexes with and without addition of HA, with the aim to dig into the influence of the different components on the structural organization and biological performance of the hybrid lipid-polymer system and correlated it with the biological behavior. In terms of particles properties, the addition of HA to the lipoplexes led to a charge inversion indicating efficient binding while maintaining colloidal stability under suitable conditions, and giving a new relevant feature to the formulation [25]. Further, the colloidally stable particles were tested for their ability to be internalized and expressed *in vitro* using THP-1 cells and human derived monocytes. With the lead systems, we then performed biodistribution and genes expression studies *in vivo* to explore the possible links between particles composition with their related physico-chemical properties and biodistribution, as well as ability to translate mRNA-coded information. These lipid-polymer hybrid complexes for nucleic acid delivery may open opportunities to shape particle properties for given therapeutic applications.

2. Material and methods

2.1. Materials

Cationic lipid 1,2-dioleoyl-3-trimethylammonium-propane (DOTAP) and helper lipid 1,2-dioleoyl-sn-glycero-3-phosphoethanolamine (DOPE), 1,2-dioleoyl-sn-glycero-3-phosphoethanolamine-N-(lissamine rhodamine B sulfonyl) (PE-Rho), 1,2-distearoyl-sn-glycero-3-phosphoethanolamine-N-diethylenetriaminepentaacetic acid (PE-DTPA), were purchased from Avanti Polar Lipids (Alabama, USA). Coatsome® SS-PalmM was obtained from NOF America Corporation (Massachusetts, USA). m1Ψ-modified, capped mRNA coding for eGFP (eGFP-mRNA), Luciferase (Luc-mRNA) and CD90.1 (Thy1.1-mRNA) were provided by BioNTech SE. EZ Cap™ Cy5-eGFP-mRNA (5-moUTP) was purchased by APExBIO Technology LLC (Texas, USA). N-(2-Hydroxyethyl)piperazine-N′-(2-ethanesulfonic acid) (HEPES) was purchased from Sigma Aldrich (Missouri, USA). Indium chloride 429 MBq (^{111}In) was purchased from Curium (Paris, France). Sodium hyaluronate (HA, weight-average molar mass, Mw = 20,000 g/mol) was purchased from Lifecore Biomedical (Minnesota, USA). Formaldehyde solution, trifluoracetic acid (TFA), and D-(+)-glucose, were provided by Sigma-Aldrich (Saint-Quentin-Fallavier, France). Sodium chloride (NaCl), hydrochloric acid (HCl) 37%, were obtained from VWR International (Fontenay-sous-Bois, France). Fluoresceinamine Isomer I, cyclohexyl isocyanide, SYBR™ Safe DNA Gel Stain, RiboRuler High Range RNA Ladder, Ultrapure™ agarose, Novex™ TBE running buffer, penicillin/streptomycin (10,000 U/mL), fetal bovine serum (FBS), sodium pyruvate, glutamine, RPMI, LIVE/DEAD™, Annexin V pacific blue™, propidium iodide (PI), Gibco™ Dulbecco's phosphate buffer saline (DPBS), Ultrapure™ DNase/RNase-Free Distilled Water, isopropanol, ethanol, chloroform, and dimethyl sulfoxide, were obtained from Thermo Fisher Scientific (Massachusetts, USA). Isoflurane USP for veterinary use was purchased from Fresenius Kabi (Ontario, Canada).

2.2. Cell lines

The naturally immortalized human monocytic cell line THP-1 is a kind gift from Prof. Vincenzo Bronte (University of Verona, Italy). Cells have been maintained in complete RPMI media (RPMI1640, heat inactivated FBS 10%, HEPES 10 mM, Penicillin-Streptomycin 50 U/mL, L-Glutamine 2 mM) with 2-β-mercaptoethanol 0.05 mM. Peripheral blood mononuclear cells (PBMCs) were isolated *via* density gradient centrifugation and cryopreserved for further use. Cryopreserved PBMCs were thawed at 37 °C in a water bath and carefully resuspended into pre-warmed human DC (hDC) medium (RPMI medium1640 (1×) + GlutaMAX-I containing 5% pooled-human-serum, 1% Sodium Pyruvate 100 mM (100×) and 1% MEM NEAA (100×)). The cells were washed (centrifugation 300 xg, 8 min, RT) once with hDC medium and total cell number was determined using the automated cell counting device ViCELL XR cell viability analyzer. 2.5 × 10^6/mL human PBMCs in hDC medium before transfection studies.

2.3. Mice

BALB/c_Rj male mice 11 weeks old purchased at Charles River Lab (Wilmington, Massachusetts, USA) were used for the *in vivo* biodistribution SPECT/CT experiments. Female BALB/c_Rj mice 11 weeks old were purchased at Janvier Labs (Le Genest-Saint-Isle, France) and used for the *in vivo* bioluminescence imaging experiments. Mice were maintained under standard conditions (12/12 h light/dark cycle, food and water *ad libitum*, 5 mice/cage). The protocols involving animals and their care were conducted in conformity with the institutional guidelines in compliance with national and international laws and policies.

2.4. Liposomes formulation and lipids quantification

Cationic liposomes (CLs) were generated by thin-film hydration method, followed by extrusion [26]. The lipids were dissolved in chloroform to generate stock solutions and then were added in a 10 mL round bottom flask to obtain a final lipid concentration of 10 mM after hydration, accordingly to molar ratios listed in Table 1. The organic solvent was removed under reduced pressure at 40 °C using a rotary evaporator (BÜCHI Rotavapor™ R-100, Île-de-France, FR). To remove the chloroform completely, the round bottom flask was let overnight in a dryer. The lipids film was rehydrated with HEPES buffer 0.1 M, pH 5.5. After 5 min of vortexing, the multilamellar vesicles were extruded through a large polycarbonate membrane (400 nm), using an Avanti mini extruder (Avanti Polar Lipids, Alabama, USA), followed by a second extrusion with a 100 nm membrane. Fluorescent liposomes were prepared with Rhodamine-labelled DOPE (PE-Rho) embedded in the liposome membrane. Rho-PE was added at a 2% mol/mol ratio to the lipid solution prior the drying process. DTPA-liposomes were prepared with PE-DTPA for radiolabeling purposes. 0.5% mol/mol of PE-DTPA was added to the lipid solution prior drying process.

Chromatographic analysis of the lipid nanoparticles' components was performed using a Waters e2695 HPLC system coupled with a Waters 2998 PDA-detector set at 203 nm. A XSelect® HSS C18 column (4.6 × 150 mm, 5 μm particle, Waters, Dublin, Ireland) was used at a temperature of 40 °C as stationary phase. The injection volume was 30 μL and the flow rate was set at 0.7 mL/min. Chromatographic separation was achieved using a gradient program involving 2 eluents, eluent A: ultrapure water +0,15% trifluoracetic acid (TFA) and eluent B: isopropanol +0,05% TFA. The analysis started with 35% eluent A and 65% eluent B. After 7 min, the mobile phase was composed of 17% eluent A and 83% eluent B and kept constant for 7 min. At 14 min, the composition was brought back to the initial state for additional 4 min. Standard curves were obtained from lipids dissolved in EtOH and linearity was assessed with a regression line by the method of least squares. Lipid components of liposomes were quantified after EtOH extraction (1:19, *v*/v) and analyses were performed in triplicates.

2.5. Fluorescent-labelled HA synthesis

The fluorescent labelled HA was synthetized accordingly to a previously reported method [27]. Briefly, 25 mg of 20 kDa HA were dissolved in 20 mL of HPW in a 50 mL round bottom flask. The HA solution was then diluted 1:2 with 20 mL of DMSO. In a glass vial 12.5 mg of fluorescein amine were dissolved in 0.25 mL of DMSO together with 12.5 μL of formaldehyde and 12.5 μL of cyclohexyl isocyanide. The latter reactant solution was added to the HA mixture, and the reaction was allowed to proceed for 5 h at room temperature in the dark at pH 4.5. The product was precipitated in ethanol containing 5 mL of saturated aqueous sodium chloride. The precipitate was centrifuged at 1500 RCF for 5 min and the supernatant discarded. The precipitation was repeated, and the final precipitate dissolved in water was allowed to dialyze against 2 L of water for 48 h through an 8–10 MWCO membrane. The final solution was then dried using a pilot freeze-dryer (Cryonext, Saint-Aunes, France).

Table 1
Lipid composition as in the patent (FR2112931) [24].

	Final lipid conc. (mM)	DOTAP conc. (mM)	DOPE conc. (mM)	ss-Palm conc. (mM)
CLs	10	5	2.5	2.5

2.6. Liposome-mRNA complexation

Lipoplexes were prepared by diluting the liposomes with RNase free water at a final concentration of 1.8 mM, and by the following addition of different mRNA concentrations (0.03–0.15 mg/mL) in RNase free water, to obtain complexes in the range 1–5 NP ratio, calculated as the mol ratio between DOTAP and nucleic acid (Table 2). The final mRNA solutions concentrations were quantified with a NanoDrop™ (Ozyme, Saint-Cyr-l'Ecole, France). HA-coated lipoplexes were prepared by the addition of 50 μL of a 0.6 mg/mL HA solution in RNase free water to the already formulated lipoplexes. For *in vivo* purposes, the lipoplexes were diluted with a solution of 10% glucose, or coated with HA dissolved in 10% glucose, to obtain the same final concentration and an appropriate osmolarity.

2.7. Characterization of liposomes and mRNA complexes

The hydrodynamic diameter distribution and surface charge of liposomes and lipoplexes were analyzed using a Malvern Zetasizer® Nano ZS (Malvern Instruments S.A., Worcestershire, UK). *Z*-average diameter (the intensity weighted mean hydrodynamic size) and polydispersity index (PDI) were determined by Dynamic Light Scattering (DLS) at a concentration of about 0.2 mg/mL. Analyses were carried out at 25 °C with an angle of detection of 173°. Zeta potential values were obtained by measuring the electrophoretic mobility of liposomes. Liposomes' stability was investigated by following the listed parameters of the systems over 28 days.

Liposomes were diluted in DPBS 10 mM to a final volume of 1 mL to assess the particles' concentration in solution by using the nanoparticle tracking analysis NanoSight NS300 (Malvern Instruments S.A., Worcestershire, UK). Ideal measurement concentrations were found by pretesting the ideal particle per frame value (20–100 particles/frame). Camera level was increased until all particles were distinctly visible not exceeding a particle signal saturation over 20%. Autofocus was adjusted to avoid indistinct particles. For each measurement, five one-minute videos were captured with a cell temperature of 25 °C and a syringe speed of 100 μL/s. After capture, the videos were analyzed with the NanoSight Software NTA 3.4 Build 3.4.003 with a detection threshold of 4.

For Cryo-TEM analysis, the liposomes and the lipoplexes formed by their complexation with mRNA, were dropped onto 300 mesh holey carbon films (Quantifoil R2/1) and quench-frozen in liquid ethane using a cryoplunge workstation (Laboratoire de Physique des Solides-LPS, Orsay, France). The specimens were then mounted on a precooled Gatan 626 sample holder, transferred into the microscope (Phillips CM120) and observed at an accelerating voltage of 120 kV.

2.8. Membrane fluidity

The membrane fluidity of the different liposomes was evaluated using Dioll, an analogue of the commercial Laurdan, an environmentally sensitive fluorescent probe. Dioll, similar to Laurdan, undergoes a change in the fluorescence intensity maximum shifting from 440 nm for a rigid membrane to 490 nm for a fluid membrane, due to the different water penetration [28]. To compare the fluidity of different systems, generalized polarization (GP) values were employed. GP values range from −1 for the most fluid, to +1 for the most condensed membranes. GP values are independent of the local probe concentrations and can be

calculated as follow:

$$GP = \frac{I(400-490)}{I(440+490)} \quad (1)$$

0.09 mM liposomes were incubated with 2 μM Dioll for 15 min before the fluorescence analysis. Then, lipoplexes were prepared as previously described. The fluorescent spectrum was recorded from 400 to 600 nm at 25 °C and 37 °C using a FP-8500 spectrofluorometer (JASCO applied science, Halifax, Canada), with an excitation wavelength set at 390 nm.

2.9. Microcalorimetric studies

The energetics of the interaction between the mRNA and the cationic liposomes was evaluated by Isothermal Titration Calorimetry (MicroCal PEAQ-ITC, Malvern). Prior the analysis, both interaction partners were dialyzed overnight at 5 °C against 10 mM HEPES buffer, degassed and equilibrated at 25 °C. 500 μM of the liposome solution was titrated with 19 successive 2 μL injections of mRNA solution (1.43 μM), the first injection was 0.4 μL and it was not considered into the result. Each injection lasted 4 s, with an interval of 150 s between successive injections. The temperature of the system was fixed at 25 °C. Control analysis was performed by the injection of mRNA into the solution buffer, following the same settings as for the titration analysis. The data were analyzed using the Microcal PEAQ-ITC 1.21 software. The thermodynamic parameters involved in the interaction, including the stoichiometry of the reaction (N), the binding constant (KD), the enthalpy (ΔH), the entropy (–TΔS), and the free energy (ΔG), were calculated by iterative curve fitting of the binding isotherms, through the two set of sites binding model.

2.10. Association studies

LRCs and HLRCs lipoplexes ranging from 1 to 5 NP ratio were prepared as described above and diluted to obtain a loading volume containing 4.58 ng of eGFP-mRNA. The agarose gel was stained with SyBRSafe for nucleotides visualization, and ran at 95 Volts for 105 min in TRIS/Borate/EDTA (TBE) buffer. Images were acquired with Invitrogen™ iBright™ FL1000 imaging system (ThermoFisher, Massachusetts, USA). Uncoated (LRC) and F-HA-coated (F-HLRC) lipoplexes ranging from 1 to 5 NP ratio were prepared as described above to obtain complexes of 10 μg/mL of Cy5-eGFP-mRNA, and measured by fluorescence correlation spectroscopy (FCS) to obtain the association degree of the fluorescent nucleic acid to the liposomes, as well as the fluorescent hyaluronic acid. Similarly, by incubating the complexes with human serum at 37 °C for 1 h, the dissociation and stability of the complexes have been studied as previously reported [29]. Briefly, fluorescence time traces were obtained by focusing a 640 nm laser line through a water-immersion lens (60× Plan Apo VC, N.A. 1.2, Nikon, Japan) 50 mm above the bottom of the glass-bottom 96-wells plate (Grainer Bio-one, Frickenhausen, Germany). The fluorescence signal obtained by using a confocal microscope (Nikon C1) was recorded by a photon counting instrument (PicoHarp 300, PicoQuant). A time trace was obtained by binning the photon counts in intervals of 60 s.

2.11. Transfection studies and cellular uptake on THP-1

A reverse transfection method was used to enhance and prolong gene expression significantly more than did the conventional method [30]. Freshly prepared lipoplexes (prepared with CLs, or Rho-CLs) at NP ratio of 1, 3, 3.5, or 5 for transfection and at NP 3 for cellular uptake studies were seeded on a 24-wells plate, and $0.15*10^6$ THP-1 cells were subsequently added in the corresponding well in 600 μL of complete media. Lipoplexes volumes were adapted in order to transfect cells with 3 μg of eGFP-mRNA for each condition. A Viromer® Red solution containing eGFP-mRNA was used as a positive control for transfection, while 3 μg of e-GFP mRNA were added to cells as negative control. Cells were incubated 24 h at 37 °C, 5% CO_2, and the medium was changed after the first 4 h to eliminate unbound lipoplexes. Cells were then washed and read on a LSR2 (BD Biosciences, California, USA) equipped with 355 nm, 405 nm, 488 nm and, 635 nm lasers. Dead cells were excluded by the analysis by using LIVE/DEAD® Stain. Data were analyzed using FlowJo™ v10.8 Software (BD Life Sciences, California, USA) and statistical analysis were performed with Prism v8.1 software (GraphPad Software, California, USA).

2.12. Transfection assay on human PBMCs

Isolated PBMCs were seeded in a 96-well plate in a volume of 80 μL. Formulations were subsequently added on top of the cell solution in one quick step and resuspended twice. The mRNA final doses were 0.5 μg, 0.25 μg, 0.1 μg, 0.05 μg, 0.02 μg and 0.01 μg per well in a volume of 20 μL. Cells and formulation were co-incubated at 37 °C and 5% CO_2 for 2 h. Transfected PBMCs were washed (centrifugation 460 x*g*, 3 min, RT) with hDC medium, resuspended in the corresponding medium and further incubated at 37 °C and 5% CO_2 for 4 h. Luciferase expression (Bright-Glo Luciferase assay, Promega, Madison, WI, USA) was measured after 6 h of total incubation.

2.13. In vitro cell viability studies

THP-1 cells were plated onto freshly prepared lipoplexes as described above and incubated for 4, 24, and 48 h at 37 °C, 5% CO_2. Medium was changed after the first 4 h. Addition of 50 μM cisplatin was used as positive cell death control. Cells were then washed and stain with Annexin V Pacific Blue™ and propidium iodide. Acquisition and statistical analysis were performed as described in the previous sections.

2.14. Time-laps microscopy

$0.15*10^6$ THP-1 cells were incubated overnight at 37 °C in a 4-well in 600 μL of complete RPMI medium. Fluorescent liposomes formulated with PE-Rho or lipoplexes were added on the plated THP-1 cells and the transfection was recorded for 24 h with LSM 880 confocal microscope (Zeiss, Oberkochen, Germany). The images were analyzed using ImageJ software.

2.15. In vivo biodistribution study of radiolabeled systems

Surface radiolabeling of liposomes was carried out by incubation of 500 μL of liposomes with 85.8 MBq (100 μL) of ^{111}In at 60 °C for 30 min. This led to an amount of radioactivity of 20.58 GBq/mmol. The molar/activity ratio was 0.24 nmol of PE-DTPA/MBq. Radiolabeling efficiency was assessed by instant thin layer chromatography on silica-gel strips (iTLC-SG, Biodex Medical Systems, Shirley, USA) using citrate buffer 100 mM pH 5 as a mobile phase. Radiochemical purity determination for evaluating free and labelled liposomes, ^{111}In activity was assessed using an ionization chamber (Capintec, Florham Park, USA). Radiochemical purity was over 97% and remained stable at least 5 days in PBS. Lipoplexes were prepared at NP ratio 2.8 for the final injection of around 4 MBq of indium (herein referred to as NP 3 for the identical characteristics). Briefly, 150 μL of radiolabeled liposomes (0.58 μmol of DOTAP) were incubated at room temperature with 0.17 nmol of mRNA (equivalent to 0.21 μmol of phosphate), for 30 min. Then, a solution of 10% glucose or 0.025 μmol HA dissolved in 10% glucose was added to the lipoplexes to adjust osmolarity. Formulations were intravenously injected into BALB/c_Rj mice under anesthesia with 3% of isoflurane. Mice received an injection of around 4 MBq ^{111}In chelated to DTPA lipoplexes, either as positively charged lipoplexes LRC, or negatively charged lipoplexes HLRC (specific activity of 20.58 and 25.77 GBq/mmol total lipid; 50 nmol total lipid/mouse in 100 μL, $n = 18$). For each formulation, groups of 3 mice were euthanized at 6 h, 24 h and 48 h

post-injection by cervical dislocation. Subsequently, organs were collected to perform a quantitative analysis of the accumulated activity. *Ex vivo* quantification of organ radioactivity was carried out with a Wizard 3″ gamma counter (Perkin Elmer, Waltham USA). For each formulation, one mouse of the 48-h group was imaged in prone position at 4 h, 24 h and 48 h. All living animal acquisitions were performed with NanoSPECT/CT™ *in vivo* animal imager (Bioscan Inc., Washington D·C, USA). During acquisition, animals were anesthetized with 1.5% of isoflurane and breathing was followed with small animal monitoring and gating system Model 1025 T (SA Instruments Inc., Stony Brook, USA). Each acquisition was performed with a preclinical SPECT/CT multiplexing with multiplexing multi-pinhole apertures. The SPECT device acquired 24 of 256 × 256 pixels for every 15°. The scan duration was 100 s per projection. The reconstruction was performed with the manufacturer software, HiSPECT, using an ordered subsets expectation maximization (OSEM) algorithm with 9 iterations and 4 subsets with an image voxel size of 0.6 mm.

2.16. In vivo transfection studies of encoding systems

LRC and HLRC formulations were obtained by mixing 4 μg of mRNA-encoding firefly luciferase (Luc-mRNA) and 4 μg of mRNA-encoding CD90.1 (Thy1.1-mRNA). 200 μL of formulations at NP 2.8 (herein referred to as NP 3) were then intravenously (i.v.) injected into BALB/c_Rj mice. Six hours later, after intraperitoneal (i.p.) injection of 150 mg/kg body weight Luciferin in PBS (XenoLight D-Luciferin potassium salt, Perkin Elmer, Rodgau, Germany), the mice were anesthetized by continuous inhalation with 2.5% isoflurane. Mice were placed in the chamber of an IVIS® Spectrum *in vivo* imaging system (Perkin Elmer, Rodgau, Germany), and bioluminescence levels were recorded at given time points. Emitted photons from live animals or extracted tissues were quantified 5 min or 15 min respectively after i.p. injection of luciferin with an exposure time of 1 min. Pictures were analyzed by IVIS® Living Image 4.0 Software and color bar represents radiance (photons s^{-1} cm^{-2} sr^{-1}).

2.17. Tissues preparation and flow cytometry

Blood was collected from the vena facialis, washed with PBS, and the erythrocytes were removed by addition of hypotonic lysis buffer with an incubation step for 3 min at room temperature. Lysis was stopped by adding an excess amount of PBS. After spin down cells were subjected to staining protocol. Spleens were stored in PBS, minced and subsequently digested with collagenase D (2 mg/mL, SigmaAldrich, Taufkirchen, Germany) for 20 min at 37 °C. Spleen-single cell suspensions were prepared mashing them through a 40 μm cell strainer (VWR International GmbH, Darmstadt, Germany) with the help of the plunger of a 5 mL syringe. Erythrocytes were removed by adding hypotonic lysis buffer and incubation for 3 min at room temperature. Lysis was stopped by adding excess amount of PBS. 2×10^6 cells were subjected to staining protocol. Monoclonal antibodies for extracellular staining included F4/80, CD8, CD19, CD11b, CD3, CD49b, CD11c, GR1 (BioLegend), PDCA1 (Miltenyi Biotec). Viability was determined using fixable viability dye (eBioSciences). Cells were stained for 20 min at 2–8 °C in the dark. Flow Cytometric Data were acquired on a Celesta FACS and analyzed with FlowJo 7.10 software (BD Life Sciences, California, USA).

2.18. Statistical analysis

All values represent mean ± SD of biological replica. Statistical tests were applied in a two- sided, unpaired fashion. One- way or two- way analysis of variance (ANOVA) followed by Tukey test for multiple comparison was performed after normality was evaluated by the Shapiro- Wilk test. The variance was similar between experimental groups in each experiment. All analyses have been performed using GraphPad Prism version 8.0. p values in panels are reported as follows: ns, $P > 0.05$; *, $P \leq 0.05$; **, $P \leq 0.01$; ***, $P \leq 0.001$; ****, $P \leq 0.0001$.

3. Results and discussion

3.1. Liposome preparation and complexation with IVT mRNA

Cationic liposomes (CLs) were prepared with a mixture of the cationic lipid DOTAP, the helper lipid DOPE, and the pH-sensitive lipid (ss-PalmM) [24]. The DOTAP/DOPE lipids combination is one of the most popular for lipoplexes formation. The addition of ionizable lipids to the mixture represent a breakthrough technology for mRNA delivery, as their selective protonation once the particles are taken up by cells, allow successful endosomal escape of its payload [31].

The liposomal hydrodynamic diameter measured by DLS was about 140 nm, with a PDI lower than 0.2 (Supplementary materials Table 1). The stability of the formulation assessed over a period of 4 months indicated that the size and the PDI remained stable (Supplementary materials Fig. 1). Similar results were obtained with rhodamine-labelled (Rho-CLs) used for cell fluorescence labelling, and DTPA-liposomes (DTPA-CLs), used for radiolabeled formulation, with a hydrodynamic size of 150 and 140 nm respectively, and a PDI lower than 0.2 in both cases. Another important parameter that can allow a better control over liposomes' final formulation is the particles' concentration, detected using nanoparticles tracking analysis (NTA). The liposomes concentration, in the order of 10^{12} particles/mL, was checked as formulation quality control for all the produced batches. The values of zeta potential (ζ-potential) of all the prepared liposome formulations were between +40 and + 55 mV, contributing to the stability of the system in aqueous media (Supplementary materials Table 1).

The DOTAP amount present in the liposomes was analyzed by RP-HPLC. Based on the obtained values, the corresponding positive charges necessary for the complexation with the genetic material (NP ratio) were quantified.

CLs were complexed with mRNA at different NP ratios, defined as the ratio of DOTAP positive amine groups (N), to negatively charged nucleic acid phosphate (P) groups. The NP character of a complex is a key parameter that can influence the surface potential, size, and stability following administration of lipoplexes. In fact, previous studies proved how the NP ratio for lipoplexes formation strongly determines the organ distribution profile of RNA expression after i.v. injection, along with the presence of different lipids interacting with the environment [32–34]. As shown in Fig. 1 A, two different families of complexes have been prepared. To obtain liposomal RNA complexes (LRCs), mRNA was mixed with liposomes at seven different NP ratios between 1 and 5. To investigate the effect of the addition of a coating agent, a defined amount of HA was subsequently mixed to the preformed LRCs to create hybrid-LRCs (HLRCs). A HA/total lipids ratio (*w*/w) of 0.5 was selected based on a previous publication [35] and a final ratio between positive and negative charges belonging to the only HA of around 1 was obtained. The polymer addition as shell after the core lipoplexes formation was meant to have an impact on the surface properties, without modifying the core characteristics of the particles. This coating offered us the possibility to study the impact of the surface modifications, without changes on the lipids composition, nor on the ratio between the genetic material and the cationic lipid, properties that both have key importance on the *in vitro* and *in vivo* behavior of the systems.

At NPs ranging between 1.5 and 2.5, both LRCs and HLRCs showed high instability, with the formation of turbid suspensions or presence of visible aggregates, as alleged from the high average size (above 1000 nm) and polydispersity values (>0.2) (Fig. 1 B, Supplementary materials Tables 2 and 3). On the contrary, for NP 1 and NPs 3 to 5, the suspensions were clear, with average particles size below 300 nm, and a PDI lower than 0.2. The recorded zeta potentials were positive for all the NPs in the case of LRCs, except for NP 1, due to mRNA excess compared to the amount of charged lipids (Fig. 1 C). On the other hand, the zeta potential of HLRCs was negative for all the tested NP ratios, as the

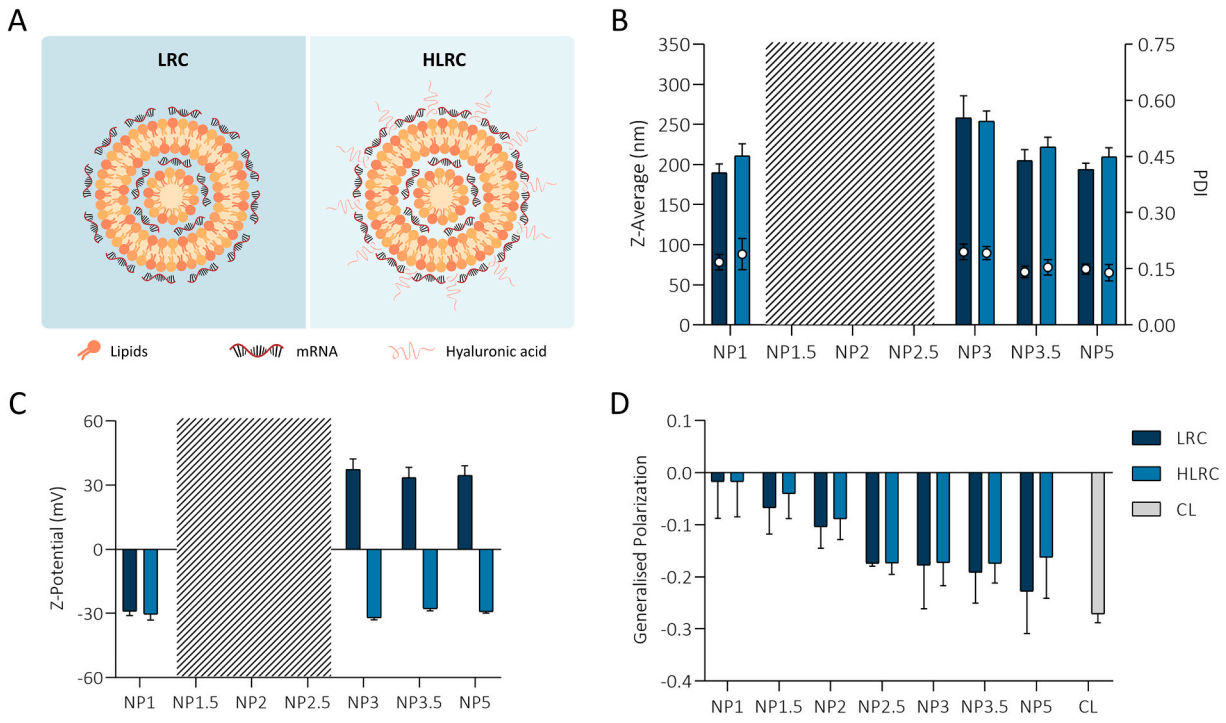

Fig. 1. Schematic illustration of the formation of LRCs and HLRCs complexes (A). Physicochemical characterization of LRCs and HLRCs in terms of size and PDI (B), surface charge (C), membrane fluidity at 37 °C (D).

hyaluronic acid coats the surface of the preformed LRCs, primarily by interacting with the free positive charges. Interestingly, while LRCs NP 1 displayed a good average size right after preparation, the initially negative ζ-potential shifted towards positive values at 24 h, accompanied by the formation of aggregates representative of the instability of the system over time (Supplementary materials Fig. 2 A). This instability was controlled once the complex at NP 1 was coated with the anionic polymer; in fact, as shown in the Supplementary materials Fig. 2 B, no differences were noticed in the samples up to six days. This might suggest how the complexation of the protective shell might play a role in helping the stability of these systems. The described structural behaviors are the answer to environment conditions, such as the pH of the complexes formation at 5.5, at which also the lipid ss-PalmM result partially protonated, and to the thermodynamic of the interactions, which is evolving with the formation of the complexes.

Table 2
NP mol ratios for lipoplexes formulation, where N refers to the mol of positive charges on the permanently cationic DOTAP, P refers to the mol of the negatively charged phosphate groups on the nucleic acid, HA to the negatively charged monomers of the polymer.

NP Ratio	LRCs		HLRCs		
	N+ (mol*10^{-8})	P- (mol*10^{-8})	N+ (mol*10^{-8})	P- (mol*10^{-8})	HA- (mol*10^{-8})
1.0	4.50	4.50	4.50	4.50	7.55
1.5	4.50	3.00	4.50	3.00	7.55
2.0	4.50	2.25	4.50	2.25	7.55
2.5	4.50	1.80	4.50	1.80	7.55
3.0	4.50	1.50	4.50	1.50	7.55
3.5	4.50	1.28	4.50	1.28	7.55
5.0	4.50	0.90	4.50	0.90	7.55

3.2. Liposomes and mRNA-complexes membrane fluidity studies

To study the impact of the nucleic acid complexation on the overall structure of the nanosystems, analyses on the fluidity of the bilayer have been performed. The degree of membrane ordering (fluidity) was quantified by using an inhouse Laurdan analogue sensitive to the polarity of the environment and thus to membrane fluidity, inserted in the liposome membrane (Dioll, patent EPO19306175.1). The probe's answer to the lipid environment can be quantified by the Generalized Polarization (GP) function defined in the paragraph 2.8 [36]. Liposomes prepared by mixing DOTAP, DOPE, and ss-PalmM resulted in a system characterized by a negative GP value of −0.27 ± 0.02 (Fig. 1 D). Increased amount of mRNA complexed with the liposome (NP 5-NP 1) led to a proportional increase of the GP values, meaning that the higher the nucleic acid content is, the more rigid is the membrane. This is probably due to a tighter interaction among the opposite charges, resulting in a more packed phase, in which the water molecules have no access to the bilayer. The fluidity of a system is often playing an important role in cell interactions and it is hypothesized that a fluid system can increase cell membrane fluidity by establishing structural defects, promoting cellular entry and endosomal escape, which are factors of key importance in defining the final efficacy of a system [37]. In particular, this parameter assisted the design of liposomes for the selective targeting towards cancer cells [38], and it may represent an additional information to select the lead formulation in gene delivery.

3.3. Morphological studies

LRCs and HLRCs are not constituted by an ordered nucleic acid phase surrounded by an external lipid bilayer, rather they are partially condensed nucleic acid complexes with an ordered substructure and irregular morphology [39]. To better investigate their structures, liposomes, LRCs and HLRCs were observed using Cryo-TEM, with appropriate films. In Supplementary materials Fig. 3 A and B, the classical morphology of the unilamellar liposomes is showed. They are spherical vesicles with an inner aqueous compartment delimited by a single bilayer membrane. The liposome interactions with mRNA and mRNA/HA are respectively reported in Fig. 2 A and B, or C and D. These pictures revealed the formation of different kinds of architectures, which has

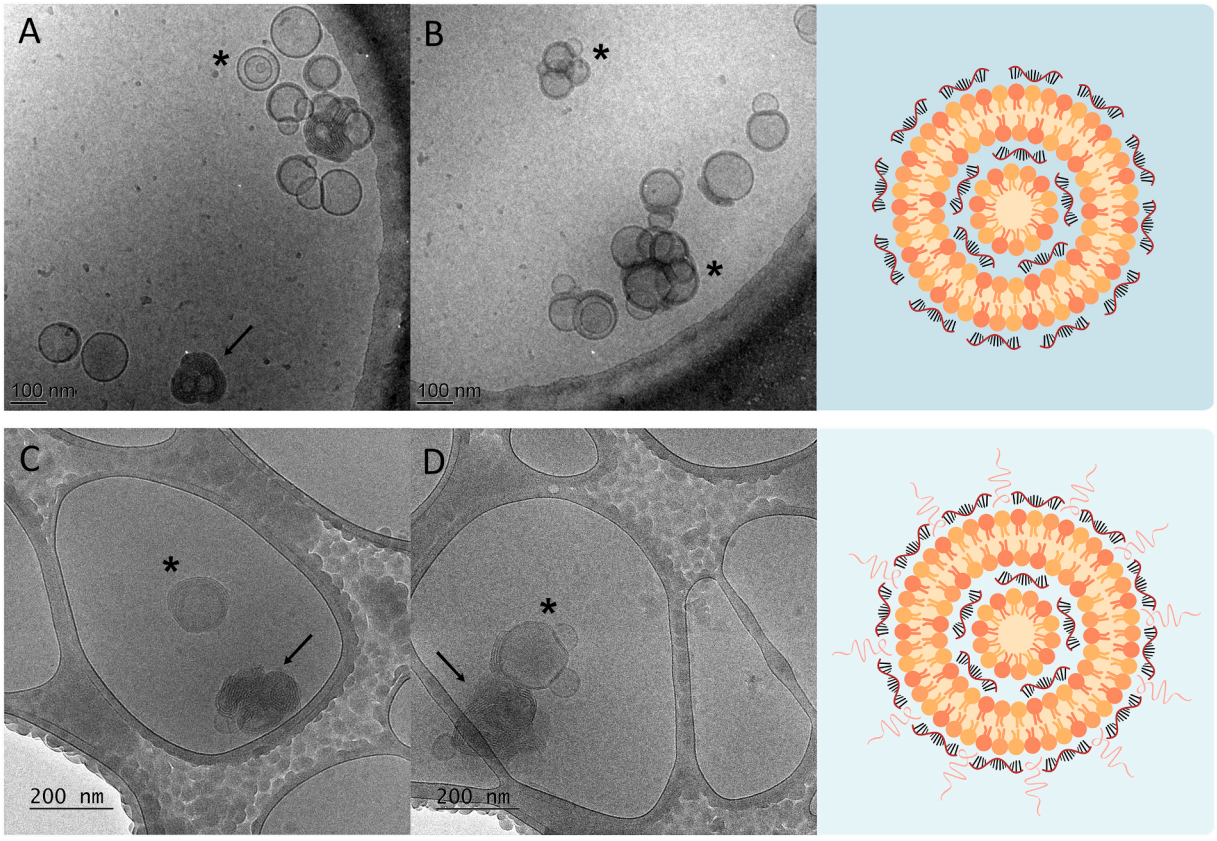

Fig. 2. Cryo-TEM images of LRCs (A and B) and HLRCs (C and D).

already been reported that can be ascribed to lipids interactions with different amounts of mRNA molecules [40]. The arrows indicate the clear multilamellar structures, whereas in correspondence of the stars other kind of organization are displayed, with a partial structuration of the nucleic acid on the liposomes' surfaces. The deformation and rearrangement of the liposomal membranes are resulting from strong electrostatic interactions between cationic lipid head groups and nucleic acid phosphate groups [39]. Liposomes absorbing to each other to form paired membranes can be regularly observed. The contact plane between the bilayers has higher contrast than their outer edges, suggesting electron-dense nucleic acid molecules (*e.g.* mRNA) acting as bridge between the membranes as already reported earlier. Also for complexes of cationic liposomes and oligonucleotides, the formation of multilamellar systems in which the alternation among nucleic acids and liposomes resemble a sandwich-like structure have been reported [41]. This structural organization is considered to be related to the protective effect of complexation on the RNA: the bilayer packing promotes the protection of the mRNA molecules from degradation better than a simple surface association, in which they would be more susceptible to degradation by serum nucleases [42]. The presence of the HA shell in Fig. 2 C and D can be highlighted by a more discontinued and less defined structure, embedded in electron-dense areas, similarly to what previously reported for hybrid complexes [43].

3.4. Liposome and mRNA interaction studies

To study the binding processes and the energetics of interaction between cationic particles and nucleic acid, microcalorimetric studies were conducted. Generally, the interaction model that mimic nucleic acid/positive lipid particles interactions consists of two processes: the electrostatic interaction between opposite charged entities, and the repulsion among them. As a result, hydration forces can cause a time-dependent rearrangement of the complex in a wide variety of macromolecular structures [44]. To describe these processes, the heat exchanged during the interaction between liposomes and mRNA was analyzed by isothermal titration calorimetry, and variations in enthalpy (ΔH) and entropy (ΔS) were obtained using computational non-linear least-squares analysis.

Figure 3 A shows the cumulative heat curves plotted against the mRNA/liposome molar ratios, with the raw data processed and fitted to obtain the thermodynamic parameters describing the interaction. As shown in the figure, the titration exhibits a biphasic structure, characterized by exothermic peaks. This profile is describing the presence of multivalent interactions, which involve the simultaneous binding of multiple ligands on one entity [45]. As summarized in Table 3 the first tendency of injections shows a trend towards increasing enthalpy until the fourth injection, corresponding to NP decreasing from 72.7 to 4.6. In this first set of binding events, the exothermic ΔH decreases, indicative of an enthalpy-driven process. This event might be related to the immediate binding of mRNA to the positively charged DOTAP. In literature the enthalpy growth has been related to the progressive incorporation of macromolecules on the positive particle surfaces [46]. Furthermore, a protonation of DOPE is contributing to increasing the ΔH value, as already proven in different studies [17]. In the second tendency (injection from 5 to 20 corresponding to NPs from 3.6 to 0.9), data start trending to a decrease in the amount of heat produced after each injection until saturation, reached at the sixth point, corresponding to NP 3. In this second set of binding events the ΔH value becomes positive, with a slight increase of the entropic component of the binding. This might be explained by the decrease in mRNA spacing and corresponding increase in mRNA-mRNA mutual repulsion. In the raw data (upper panel) it is important to notice a segmented baseline which indicates a non-reversable binding event, due to the complexes precipitation in the instability range of the systems. It is known from structural studies that the nucleic acid spacing is constant until the tightest possible packing of the strands in the complex. Accordingly, no more mRNA can

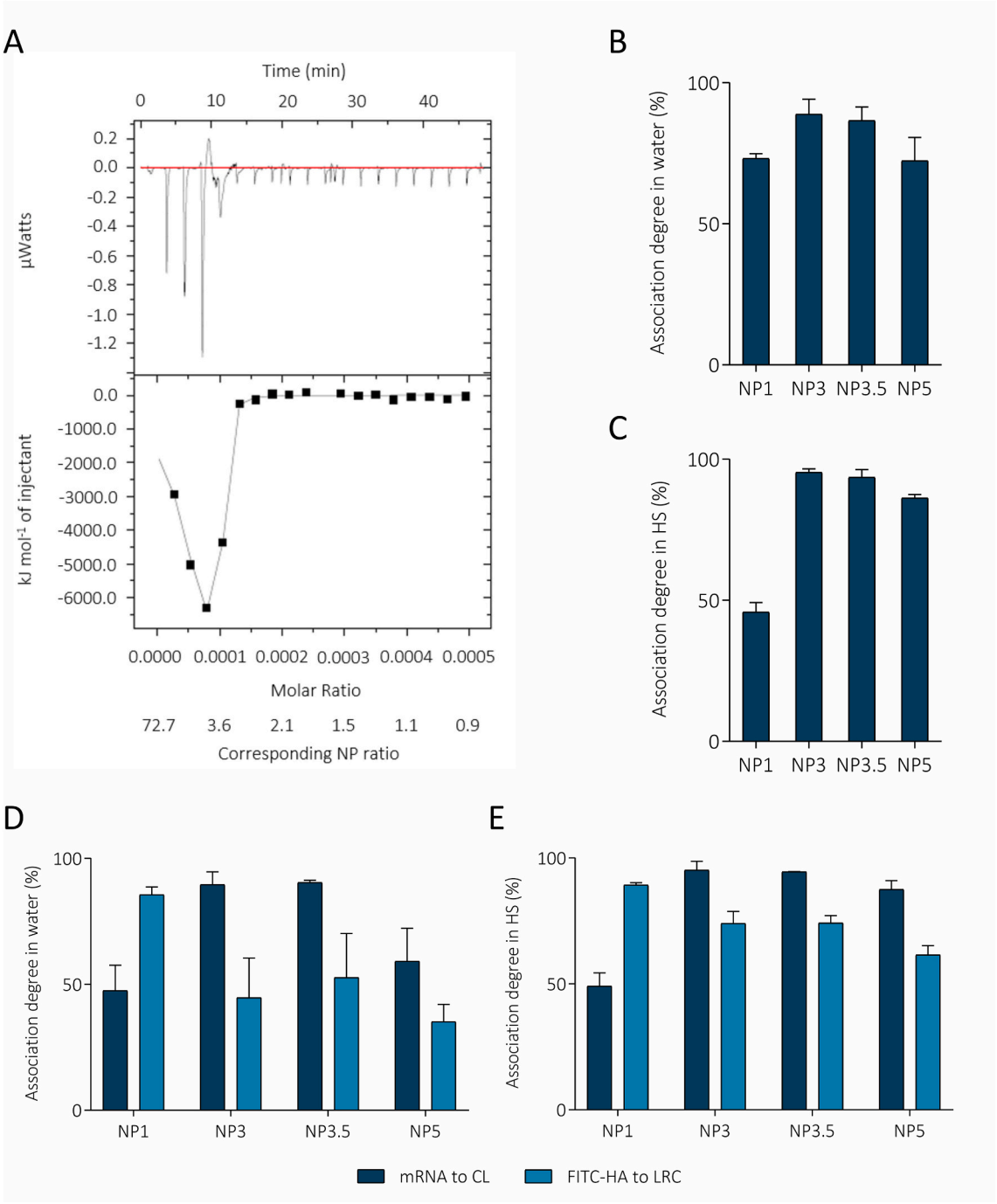

Fig. 3. ITC profile of the association between the cationic liposome and mRNA. In the upper part, raw data (after baseline subtraction) obtained from the titration of liposomes (500 µM) with mRNA (1.43 µM) in 10 mM HEPES buffer at 25 °C are shown, displaying the calorimetric response peaks in µWatt during progressive injections of the macromolecule, as well as the corresponding NP ratios. In the lower part, the data are representing the binding enthalpies corrected for heat of ligand injection. The solid line represents the fitting of the two set of sites model (A). FCS experiments showing Cy5-mRNA association degree in buffer (B) and in HS (C) to the liposomes, representing LRCs systems. FCS experiments displaying Cy5-mRNA and Fluo-HA association in buffer (D) and HS (E) to the liposomes, representing HLRCs.

Table 3
Thermodynamic values describing the liposome/IVT-mRNA interactions.

Events	NP ratio range	ΔH (cal/mol)	ΔS (cal/mol/deg)	ΔG (cal)
1st (Inj. 1–4)	72.7–4.6	$-5.64*10^3$	$-1.89*10^1$	$-1.58*10^1$
2nd (Inj. 5–20)	3.6–0.9	$3.39*10^4$	$1.14*10^2$	$-5.20*10^1$

subsequently bind to the complex without a complex rearrangement happening over a time which is not possible to represent over an ITC measurement. In this titration, this surface saturation sets the upper limit for the calorimetric endpoint, which depends on aggregation and is determined by the point where complex particles cannot readily accommodate additional material [47].

3.5. mRNA-Liposomes association and stability studies

To assess the complexation of LRCs and HLRCs, electrophoretic assays were performed at all the studied NP ratios. In the case of LRCs, a weak signal corresponding to free mRNA was seen for NP 1 (Supplementary materials Fig. 4, line 3), representative of the exceeding mRNA. On the other hand, in the presence of hyaluronic acid-coating, no fluorescence was observed (Supplementary materials Fig. 5, line 3). This result supports the DLS data, which showed the instability of LRC NP 1 after 24 h due to the excess of unbound mRNA molecules, but that was not observed for HLRC NP 1. Both these results suggest the participation of HA to the complexes stabilization. For all the other complexes, no unbound mRNA was visible, suggesting a strong interaction taking place between the liposome and the nucleic acid (Supplementary materials Fig. 4 and 5, lines 4–9).

Gel electrophoresis is not applicable to follow degradation in biological media due to the high background signal of macromolecules present in the biological samples. To study particles' stability, fluorescence correlation spectroscopy (FCS) analyses were performed. FCS is a microscopy-based technique that monitors the fluorescence intensity fluctuations of molecules diffusing in and out of the focal volume of a confocal microscope. By analyzing the fluctuations of fluorescence intensity over time, FCS allowed the determination of the concentration of intact mRNA in a simple dilution series based on single species fit to the auto-correlation curve [29]. Within a short time, when free mRNA molecules are present in the focal volume, a fluorescence signal proportional to the local mRNA concentration (baseline) is obtained. When the mRNA is complexed with lipid-polymer hybrid nanoparticles, the concentration of free mRNA (*e.g.* the baseline) drops, and high intensity fluorescence peaks appear each time a nanocomplex containing fluorescent mRNA molecules passes the detection volume. Conversely, when mRNA dissociates from the complexes, the concentration of free mRNA increases, resulting in an increase of the baseline. The variation in the intensity of the baseline can be used to calculate the percentage of complexed/free mRNA [48]. Here, Cy5-labelled mRNA was used to monitor the fluorescence intensity of the intact nucleic acid, together with fluoresceinamine-labelled HA (Fluo-HA) for the coating of HLRCs, synthetized as described in paragraph 2.5, and schematized in Supplementary materials Fig. 6. The reaction for the preparation of Fluo-HA led to a recovery yield of 96%, with a labelling efficiency of about 45%.

Different NP ratios (1, 3, 3.5 and 5) of LRCs were analyzed to quantify the mRNA complexed with the lipids after formulation, and also after 1 h of incubation in undiluted human serum (HS) at 37 °C to mimic the conditions after intravenous (i.v.) injection (Supplementary materials Fig. 7 and 8). The same analyses were conducted to detect not only the Cy5-mRNA, but also the fluorescent shell of HA added after the mRNA/lipid core formation, as shown in Supplementary materials Fig. 9 and 10.

Figure 3 B shows the association degree between Cy5-eGFP-mRNA and liposomes. Respectively, 73.2, 88.9, 86.6, and 72.4% of the mRNA initially added is associated in NP 1, NP 3, NP 3.5, and NP 5 complexes. These data are qualitatively in agreement with those obtained by electrophoresis. At NP > 1 mRNA is complexing with liposomes. At NP 5 we can observe a slight decrease in the complexation degree, but as previously explained by Zhang et al., the interpretation of the fluctuation profiles (Supplementary materials Fig. 7, 8, 9 and 10) suggests that this might be due to a different organization of mRNA with the lipid particles and not to an actual decomplexation as in the case of NP 1 [49]. Next, the ability of complexes to retain the complexed mRNA in the presence of human serum was evaluated (Fig. 3 C). 95.4, 93.6, and 86.3% of the mRNA was retained at NP 3, NP 3.5 and NP 5, respectively. In the case of NP 1, only 45.8% of the nucleic acid held on, probably due to the excess of mRNA present in the complex, which, as reported in the DLS measurements, leads to a progressive instability. This instability can be explained by the presence of an excess of genetic material directly exposed to the environment, which interacts with the serum proteins. The same set of experiments has been conducted on HLRCs, by complexing Fluo-HA, together with the one of Cy5-eGFP-mRNA (Fig. 3 D and E). Concerning the stability of these complexes, the results show similar behaviors than those obtained for LRC regarding the mRNA association. In fact, it is here proved that the presence of the anionic polymer is not impairing the mRNA complexation in both water and HS (Fig. 3 D and E). In the case of NP 3, NP 3.5, and NP 5, the amount of HA binding to the complexes' surface in water was 44.7, 52.7, and 35.2% respectively. It is interesting to note the case of NP 1, in which the mRNA complexation seems much poorer when compared to the one of hyaluronic acid (around 85.6%). HA might be able to cover the complex surface efficiently as showed by these results, by forming different kinds of interactions, thus improving the stability of the system (see DLS data, Fig. 1 B and gel electrophoresis, Supplementary materials Fig. 4 and 5). Concerning HS, NP 3, 3.5, and 5 behaviors are very similar between each other, with an association of 74.1, 74.2, and 61.5% respectively of the coating polymer.

Overall, all the systems except NP 1 LRC and HLRC can form stable complexes with both the genetic material and the shell polymer, not only in the optimized formulation conditions, but also in the presence of human serum. The results obtained in HS are important to have a consistent proof of the stability of the systems upon injection in the bloodstream.

3.6. Transfection and viability studies

The ability of LRCs and HLRCs to efficiently enter cells was firstly evaluated with THP-1 cells. THP-1 is a spontaneously immortalized monocyte-like cell line which represents a valuable tool for investigating monocyte biology and function in both healthy and pathological situations [50]. eGFP was used as reporter protein to monitor mRNA transfection efficiency. As determined by FACS analysis (Fig. 4 A and B), after 24 h of incubation eGFP expression was obtained with all the NP tested with no significant difference between the LRCs and HLRCs. Cell viability of transfected cells is reported in Supplementary materials Fig. 11 and it shows that all the transfected cells displayed a cell viability level above 70%, which represented the minimum acceptable [51]. LRCs and HLRCs prepared at NP 3 showed a higher eGFP-positivity than NP 3.5 ($*p = 0.016$ for LRC and $****p < 0.0001$ for HLRC) and NP 5 (****p < 0.0001 for both LRC and HLRC). Even if there is no significative difference between NP 1 and NP 3 in terms of eGFP expression, NP 1 LRC were highly unstable 24 h after formulation and, in addition, the two complexes at NP 3 showed the higher fluorescence intensity, as displayed in the panels. For these reasons, LRCs and HLRCs at NP 3 were selected for the further studies.

The assessment of cell death was performed using AnnexinV-PI test upon incubation of NP 3 lipoplexes until 48 h. As shown in Supplementary material Fig. 12, there are no significant differences in the viability at 4 and 24 h. At 48 h, the percentage of living cells is higher than 85% in both LRCs and HLRCs, while the control reduced cell viability below 75% and increased late and early apoptosis.

Luciferase was used as reporter protein to monitor mRNAs transfection efficiency in human derived monocytes treated with LRC and HLRC at NP 3, and quantified (Supplementary materials Fig. 13 A). A substantial luminescence signal was found in cells treated with the lowest amount of Luc-mRNA (0.01 μg), and it was augmenting at increasing concentrations of the lipoplexes up to 0.1 μg. Starting from 0.25 μg, the signal was reduced probably due to a reduced cells viability (Supplementary materials Fig. 13 B). This experiment represents an important proof-of-concept of the transferability of the transfection ability of both hybrid and classic particles on human derived cells.

3.7. Cellular uptake of LRCs and HLRCs

To determine the nanoparticles' internalization kinetics, Rhodamine-PE lipid was incorporated into the liposome membranes.

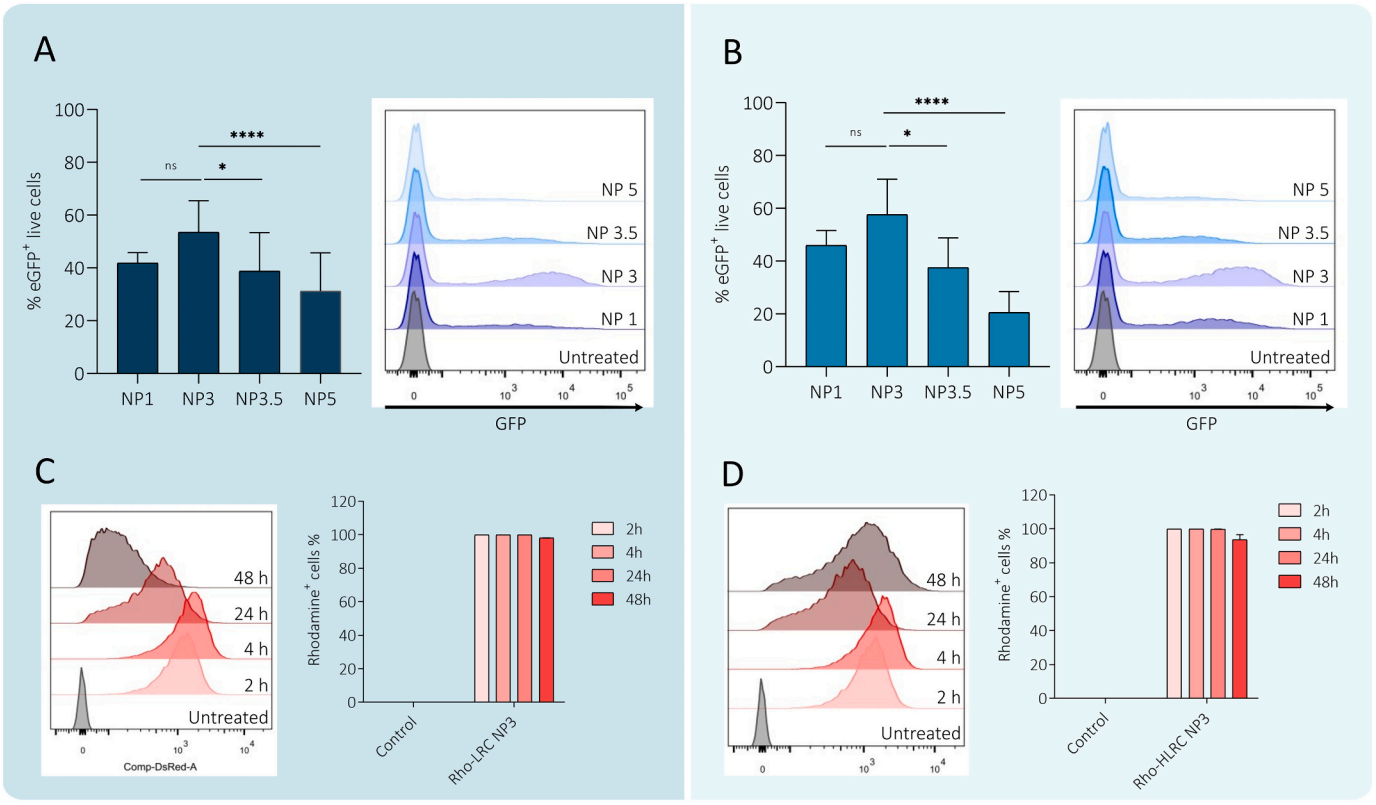

Fig. 4. Transfection efficiency, cell viability and internalization of THP-1 cells after transfection with lipid nanoparticles complexed with eGFP at different NP ratios. Flow cytometry analysis of transfection efficiency and fluorescence intensity of THP-1 monocytes with LRCs (A) and HLRCs (B) at different NP ratios (1, 3, 3.5 and 5) after 24 h. The internalization of LRC NP 3 (C) and HLRC NP 3 (D) in THP-1 cells measured at indicated time points (2, 4, 24, and 48 h) with flow cytometry using rhodamine fluorescent CLs for complexation.

Rhodamine-LRC and -HLRC were obtained with eGFP-mRNA at NP 3 to follow their internalization and the delay in mRNA translation in the cytoplasm of THP-1 cells. Both fluorescent signals were observed with flow cytometry at 2, 4, 24 and 48 h after transfection. At 2 h, Rhodamine-LRCs and HLRCs were detected in all the live cells using FACS analysis (Fig. 4 C and D). Rhodamine fluorescent signal was clearly detectable at each time point, with a slight decrease for both LRCs and HLRCs after 48 h, suggesting the initiation of the nanoparticle externalization from cells. Rhodamine MFI values for the cell populations described in Fig. 4 C and D are shown in Supplementary materials Fig. 14. The MFI intensity is comparable between LRC and HLRC, indicating a similar ability of both nanoparticles to bind and be internalized by THP-1 cells, and suggesting that the addition of hyaluronic acid does not alter the nanoparticle binding properties on this cell line. These data indicate that both LRC and HLRC NP 3 have similar cellular accumulation and internalization kinetics, with both nanoparticles showing maximum accumulation 4 h after initial incubation with cells. The reduction in rhodamine intensity from 24 h suggests that the rate of degradation or extracellular release of rhodamine is greater than the acquisition of new molecules through nanoparticle internalization. To confirm the actual internalization of the fluorescent-labelled complexes, simultaneous eGFP expression was evaluated. Among the living cells, almost the totality was either internalizing, either interacting at the surface level with the nanoparticles, and around 60% of these cells were expressing eGFP. These results coupled together are suggesting a preponderant particles internalization in THP-1 cells. In addition, time laps video shows that eGFP expression starts after 5 h of incubation and increased until 24 h (Videos).

3.8. *In vivo biodistribution and bioluminescence studies*

After confirming the feasibility of lipoplexes transfection in cell culture, the targeting of the delivery systems on organ level was determined after intravenous injection of ^{111}In-labelled NP 3 in BALB/c_Rj mice. SPECT/CT imaging was performed at 6, 24, and 48 h after injection with a dose corresponding to about 4 MBq. For both LRCs and HLRCs, clear images were obtained, with a visual particle accumulation in the liver and spleen (Fig. 5 A and B, Supplementary materials Fig. 15 A and C).

The amount of radioactivity of each animal organ was quantified with a gamma counter and normalized and presented as a percentage of injected dose per gram of tissue (%/ID/g) (Fig. 5 C and D, Supplementary material Fig. 15 B and D). This confirmed that nanoparticles biodistribution did not significantly differ between LRC NP 3 and HLRC NP 3. Lipid nanoparticles easily accumulate in the liver after intravenous injection because of its well-perfused nature, and thanks to the fenestration in the liver endothelium. At 6 h post injection, in both cases the percentage of particles accumulated in the reticuloendothelial system (RES) were equally distributed in the liver and spleen, with respectively 47.0 and 44.1% of the ID/g for LRC, and 44.5 and 39.9% of the ID/g for HLRC. At 24 h, in both cases the ID/g was increasing in the spleen, while decreasing in the liver. At this time point, 29.5% of the ID/g were detected in the liver and 58.9% in the spleen for LRC, whereas these values were 37.2% and 52.4% respectively for HLRC. The values obtained maintained the same pattern at 48 h, with 39.1 and 52.4 for LRC, and 30.5 and 57.2% for HLRC respectively in liver and spleen.

In addition to the biodistribution of indium-chelated lipoplexes, it is important to understand the *in vivo* translation ability of mRNA delivered *via* LRCs and HLRCs. Therefore, mRNA lipoplexes at NP 3 were prepared by complexing firefly luciferase mRNA (Luc-mRNA) in

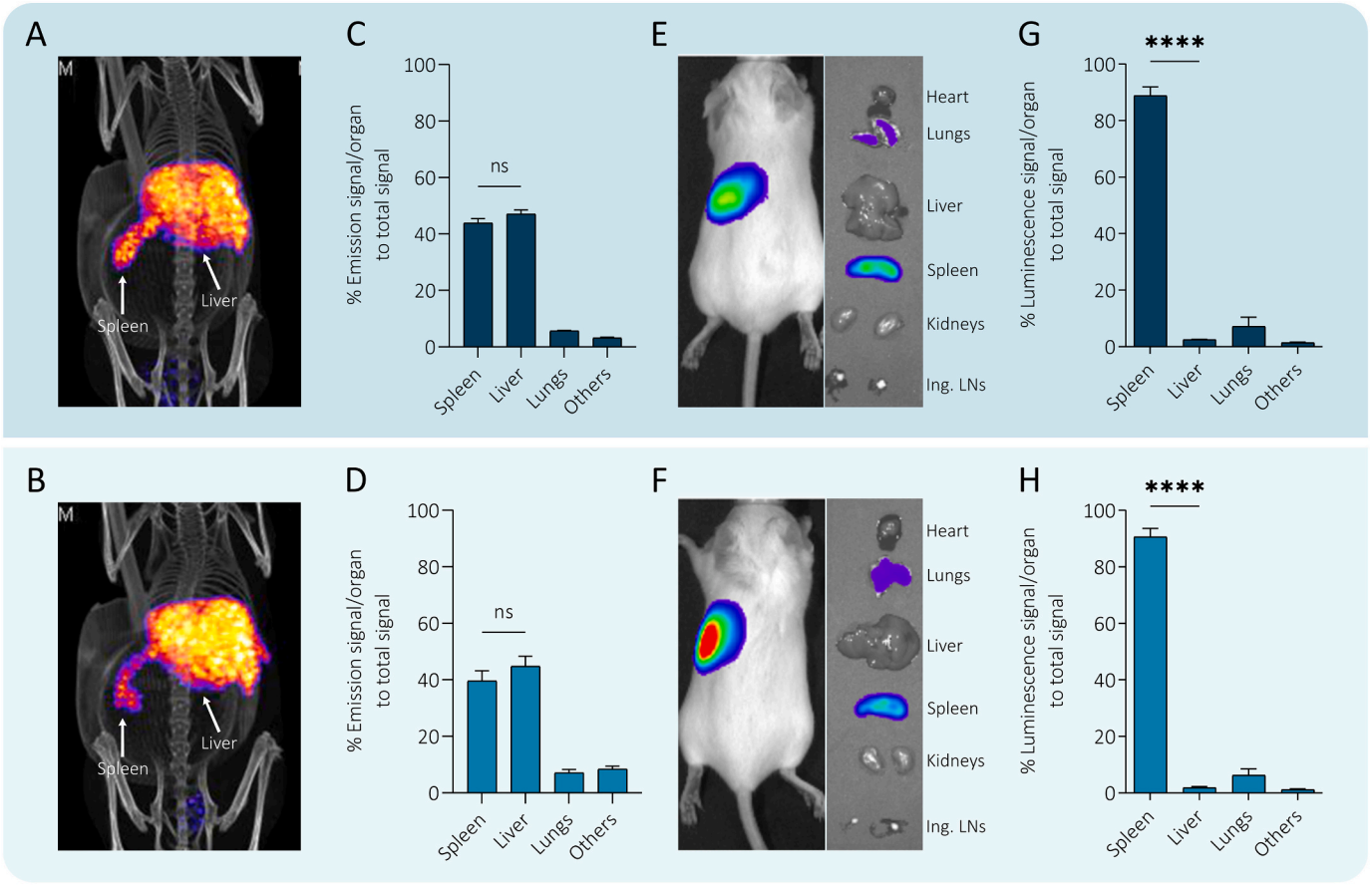

Fig. 5. MicroSPECT/CT images of ^{111}In-LRC NP 3 (A) and ^{111}In-HLRC NP 3 (B) at 6 h after the injection to visualize the targeting properties of the radiolabeled formulations. Quantitative biodistribution for LRC (C) and HLRC (D) at 6 h after intravenous injection in BALB/c_Rj mice expressed as percentage of injected dose per gram of tissue ($n = 3$). Bioluminescence images of BALB/c_Rj mice *in vivo* and of the explanted organs for LRC (E) and HLRC (F). Quantitative bioluminescence signal per organ for LRC (G) and HLRC (H) (n = 3).

combination with CD90.1 mRNA (Thy1.1-mRNA) and i.v. injected. Compared to control mice injected with Luc-mRNA, both positively and negatively charged lipoplexes produced well detectable bioluminescence signals (Supplementary materials Fig. 16). The images shown in Fig. 5 E and F represent the emitted photons from live animals and extracted tissues at 6 h. Fig. 5 G and H are a quantitative representation of the percentage of luminescence signal in the different organs normalized by the total signal. As stated in the results, no difference was reported between the two systems at 6 h, indicating that both LRC and HLRC present similar gene translation ability highly prevalent at spleen level, being of 88.6% and 90.0% for LRC and HLRC respectively. At 24 h, lower bioluminescence signal was detected reaching a signal close to the background noise 48 h after injection (data not shown), meaning that the mRNA was cleared or degraded as expected, while the radiolabeled system, representing the fate of the lipid components of the delivery system, was still recovered up to 48 h.

When comparing the biodistribution profile referred to the radiolabeled lipid systems with the bioluminescence signal related to the *in vivo* protein expression at 6 h, we can conclude that even if both formulations are rapidly accumulating in the liver and the spleen (Fig. 5 C and D), the protein translation occurs only in the spleen (Fig. 5 G and H). These results were not of surprise and were previously described by other authors. Meyer et al. already reported this discrepancy by following a fluorescent-labelled mRNA and its transfection efficiency *in vivo* [52]. They stated a preferential accumulation in the liver but a protein expression mainly in the spleen or lungs, depending by the amount of DOTAP incorporated in the system. Similarly, Cheng et al. studied the impact of differently charged lipids to i.v. injected lipid particles with validated transfection efficacy in hepatocytes [33]. They showed that an increasing amount of DOTAP was shifting the protein expression from the liver to the spleen, and then to the lung, proving that the DOTAP percentage in the formulation was the key factor tuning tissue specificity. These results were in line with what previously highlighted also by Rosigkeit et al. [34]. Here, the comparable behavior of LRC and HA-coated particles *in vivo* shows that the presence of the anionic polymers on the system surface at the specific reported conditions seems not affecting the possible bindings or interactions happening in the bloodstream, in which the coating resulted steady bound (Fig. 3 C and E). The biodistribution in first place, and after that the protein translation in the healthy mice models used for the studies result a direct consequence of the lipid composition.

A deeper characterization of nanoparticles targeting properties on cellular level has been performed by analysis of their transfection abilities of different immune cell subsets in the spleen of LRC and HLRC injected mice. The expression of membrane receptor CD90.1, encoded by the mRNA, has been used to identify the cells able to efficiently uptake and translate the complexed mRNA (gating details on Supplementary materials Fig. 17). Among the different immune populations commonly found in the spleen, macrophages were distinguished to be the main targeted cells of both LRCs and HA-coated particles whereas other populations of both lymphoid and myeloid lineage, showed no or very little expression of CD90.1 (Fig. 6). The ability of these nanosystems to preferentially transfect macrophages could represent a desirable feature since the widely implications that these cells have in a multitude of pathologies and immune-mediated mechanisms. To cite an example, macrophages are considered a major target in cancer therapy

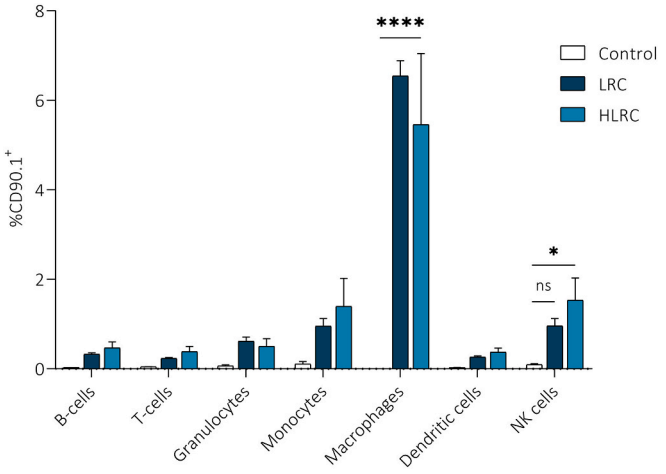

Fig. 6. Expression of the reporter gene measured by flow cytometry in splenic immune cell subsets 6 h after i.v. injection of 4 μg Thy1.1 mRNA complexed in LRC and HLRC NP 3.

due to their ability to either favor or hindered tumor progression depending on their polarization state [53]. Beside cancer, macrophages are key players in tissue homeostasis and in the promotion or resolution of any inflammatory responses and their activation leads both tissue damage and repair [54].

The late available literature is widely describing the *in vivo* fate of lipid-based nanosystems [32–34]. Our findings are adding important details on how modification of lipoplexes to obtain hybrid composites is preserving the characteristics and the behaviors of the original lipid particle, facilitating the design of tailored systems.

4. Conclusions

In our work we designed and characterized lipid-polymer hybrid particles by correlating physico-chemical properties and biological fate *in vitro* and *in vivo*. Optimized systems were obtained from studying critical formulation parameters as mRNA complexation and nanoparticles stability both in cell culture and in complex medium as serum. Lipid composition and lipid/mRNA ratio were the driving forces for nanoparticles architecture and consequent distribution *in vivo*. Assembly of a polymeric shell to a core lipoplex allowed controlled modification of physicochemical parameters such as charge, providing options to modulate stability and surface functionality, without affecting the core properties of the lipid/mRNA system.

Supplementary data to this article can be found online at https://doi.org/10.1016/j.jconrel.2022.11.042.

Animal studies

Animal experiments were approved by the local animal ethics of University Claude Bernard Lyon 1 and carried out in compliance with current French guidelines (APAFIS#28887) or by local authorities of Rhineland-Palatine, Landesuntersuchungsamt Koblenz, Germany (G15-12-078).

CRediT authorship contribution statement

Valentina Andretto: Methodology, Investigation, Writing – original draft. **Mathieu Repellin:** Methodology, Visualization, Formal analysis, Writing – review & editing. **Marine Pujol:** Methodology, Visualization, Formal analysis, Writing – review & editing. **Eyad Almouazen:** Methodology, Visualization, Formal analysis, Writing – review & editing. **Jacqueline Sidi-Boumedine:** Methodology, Visualization, Formal analysis, Writing – review & editing. **Thierry Granjon:** Methodology, Visualization, Formal analysis, Writing – review & editing. **Heyang Zhang:** Methodology, Visualization, Formal analysis, Writing – review & editing. **Katrien Remaut:** Methodology, Visualization, Formal analysis, Writing – review & editing. **Lars Petter Jordheim:** Methodology, Visualization, Formal analysis, Writing – review & editing. **Stéphanie Briançon:** Methodology, Visualization, Formal analysis, Writing – review & editing. **Isabel Sofia Keil:** Methodology, Visualization, Formal analysis, Writing – review & editing. **Fulvia Vascotto:** Data curation, Formal analysis, Writing – review & editing, Resources, Conceptualization. **Kerstin C. Walzer:** Data curation, Formal analysis, Writing – review & editing, Resources, Conceptualization. **Ugur Sahin:** Data curation, Formal analysis, Writing – review & editing, Resources, Conceptualization. **Heinrich Haas:** Data curation, Formal analysis, Writing – review & editing, Resources, Conceptualization. **David Kryza:** Data curation, Formal analysis, Writing – review & editing, Resources, Conceptualization. **Giovanna Lollo:** Data curation, Formal analysis, Writing – review & editing, Resources, Conceptualization.

Declaration of Competing Interest

The authors declare that they have no known competing financial interests or personal relationships that could have appeared to influence the work reported in this paper.

Data availability

Data will be made available on request.

Acknowledgements

Euronanomed III (Joint Translational Call 2017, Project RESOLVE ANR-17-ENM3-0008-02); COST Action CA 17140 “Cancer Nanomedicine from the Bench to the Bedside” supported by COST (European Cooperation in Science and Technology); IDEXLYON Project of the University of Lyon (Programme Investissements d’Avenir, ANR-16-IDEX-0005) Arqus, ANR project NanoImmune.

References

[1] J. Buck, P. Grossen, P.R. Cullis, J. Huwyler, D. Witzigmann, Lipid-based DNA therapeutics: hallmarks of non-viral gene delivery, ACS Nano 13 (2019) 3754–3782, https://doi.org/10.1021/acsnano.8b07858.
[2] K.A. Hajj, K.A. Whitehead, Tools for translation: non-viral materials for therapeutic mRNA delivery, Nat. Rev. Mater. 2 (2017) 1–17, https://doi.org/10.1038/natrevmats.2017.56.
[3] T. Niidome, L. Huang, Gene therapy progress and prospects: nonviral vectors, Gene Ther. 9 (2002) 1647–1652, https://doi.org/10.1038/sj.gt.3301923.
[4] A. Wicki, D. Witzigmann, V. Balasubramanian, J. Huwyler, Nanomedicine in cancer therapy: challenges, opportunities, and clinical applications, J. Control. Release 200 (2015) 138–157, https://doi.org/10.1016/j.jconrel.2014.12.030.
[5] H. Yin, R.L. Kanasty, A.A. Eltoukhy, A.J. Vegas, J.R. Dorkin, D.G. Anderson, Non-viral vectors for gene-based therapy, Nat. Rev. Genet. 15 (2014) 541–555, https://doi.org/10.1038/nrg3763.
[6] O. Boussif, F. Lezoualc’h, M.A. Zanta, M.D. Mergny, D. Scherman, B. Demeneix, et al., A versatile vector for gene and oligonucleotide transfer into cells in culture and in vivo: Polyethylenimine, Proc. Natl. Acad. Sci. U. S. A. 92 (1995) 7297–7301, https://doi.org/10.1073/pnas.92.16.7297.
[7] A.K. Patel, J.C. Kaczmarek, S. Bose, K.J. Kauffman, F. Mir, M.W. Heartlein, et al., Inhaled Nanoformulated mRNA Polyplexes for protein production in lung epithelium, Adv. Mater. 31 (2019) 1805116, https://doi.org/10.1002/adma.201805116.
[8] C.D. Siewert, H. Haas, V. Cornet, S.S. Nogueira, T. Nawroth, L. Uebbing, et al., Hybrid biopolymer and lipid nanoparticles with improved transfection efficacy for mRNA, Mol. Ther. 9 (2020) 1509–1519, https://doi.org/10.3390/cells9092034.
[9] A. Akinc, M.A. Maier, M. Manoharan, K. Fitzgerald, M. Jayaraman, S. Barros, et al., The Onpattro story and the clinical translation of nanomedicines containing nucleic acid-based drugs, Nat. Res. Forum 14 (2019), https://doi.org/10.1038/s41565-019-0591-y.
[10] F.P. Polack, S.J. Thomas, N. Kitchin, J. Absalon, A. Gurtman, S. Lockhart, et al., Safety and efficacy of the BNT162b2 mRNA Covid-19 vaccine, N. Engl. J. Med. 383 (2020) 2603–2615, https://doi.org/10.1056/nejmoa2034577.
[11] L.R. Baden, H.M. El Sahly, B. Essink, K. Kotloff, S. Frey, R. Novak, et al., Efficacy and safety of the mRNA-1273 SARS-CoV-2 vaccine, N. Engl. J. Med. 384 (2021) 403–416, https://doi.org/10.1056/nejmoa2035389.

[12] S. Bochicchio, G. Lamberti, A.A. Barba, Polymer–lipid pharmaceutical nanocarriers: innovations by new formulations and production technologies, Pharmaceutics 13 (2021) 1–15, https://doi.org/10.3390/pharmaceutics13020198.

[13] X. Cheng, R.J. Lee, The role of helper lipids in lipid nanoparticles (LNPs) designed for oligonucleotide delivery, Adv. Drug Deliv. Rev. 99 (2016) 129–137, https://doi.org/10.1016/j.addr.2016.01.022.

[14] T.T.H. Thi, E.H. Pilkington, D.H. Nguyen, J.S. Lee, K.D. Park, N.P. Truong, The importance of poly(ethylene glycol) alternatives for overcoming PEG immunogenicity in drug delivery and bioconjugation, Polymers (Basel) 12 (2020) 298, https://doi.org/10.3390/polym12020298.

[15] J. Devoldere, M. Wels, K. Peynshaert, H. Dewitte, S.C. De Smedt, K. Remaut, The obstacle course to the inner retina: hyaluronic acid-coated lipoplexes cross the vitreous but fail to overcome the inner limiting membrane, Eur. J. Pharm. Biopharm. 141 (2019) 161–171, https://doi.org/10.1016/j.ejpb.2019.05.023.

[16] A.P.B. Almeida, G.B.R. Damaceno, A.F. Carneiro, A. Bohr, H.R. Gonçalves, M. C. Valadares, et al., Mucopenetrating lipoplexes modified with PEG and hyaluronic acid for CD44-targeted local siRNA delivery to the lungs, J. Biomater. Appl. 34 (2019) 617–630, https://doi.org/10.1177/0885328219863291.

[17] T.L. Nascimento, H. Hillaireau, M. Noiray, C. Bourgaux, S. Arpicco, G. Pehau-Arnaudet, et al., Supramolecular organization and siRNA binding of hyaluronic acid-coated Lipoplexes for targeted delivery to the CD44 receptor, Langmuir 31 (2015) 11186–11194, https://doi.org/10.1021/acs.langmuir.5b01979.

[18] M.C. Hamoudi, E. Henry, N. Zerrouk, D. Scherman, P. Arnaud, E. Deprez, et al., Enhancement of siRNA lipid-based vector stability and siRNA integrity in human serum with addition of anionic polymer adjuvant, J. Drug Deliv. Sci. Technol. 26 (2015) 1–9, https://doi.org/10.1016/j.jddst.2015.01.001.

[19] A.R. Jordan, R.R. Racine, M.J.P. Hennig, V.B. Lokeshwar, The role of CD44 in disease pathophysiology and targeted treatment, Front. Immunol. 6 (2015) 182, https://doi.org/10.3389/fimmu.2015.00182.

[20] H. Kim, H. Jeong, S. Han, S. Beack, B.W. Hwang, M. Shin, et al., Hyaluronate and its derivatives for customized biomedical applications, Biomaterials 123 (2017) 155–171, https://doi.org/10.1016/j.biomaterials.2017.01.029.

[21] P.S. Kowalski, A. Rudra, L. Miao, D.G. Anderson, Delivering the messenger: advances in Technologies for Therapeutic mRNA delivery, Mol. Ther. 27 (2019) 710–728, https://doi.org/10.1016/j.ymthe.2019.02.012.

[22] Du Z, Munye M, Tagalakis A, Reports MM-S, 2014 undefined. The role of the helper lipid on the DNA transfection efficiency of lipopolyplex formulations. NatureCom (2014) 4:7107. https://doi.org/10.1038/srep07107.

[23] H. Akita, Development of an SS-Cleavable pH-activated lipid-like material (ssPalm) as a nucleic acid delivery device, Pharmaceut. Soc. Jpn. vol. 43 (2020), https://doi.org/10.1248/bpb.b20-00534.

[24] G. Lollo, E. Almouazen, D. Kryza, V. Andretto, M. Repellin, L. Schaeffer, A.B. S. Jacquier, Nanoparticles for nucleic acid delivery, FR2112931 (2021).

[25] A. Mero, M. Campisi, Hyaluronic acid bioconjugates for the delivery of bioactive molecules, Polymers (Basel) 6 (2014) 346–369, https://doi.org/10.3390/polym6020346.

[26] H. Zhang, Thin-film hydration followed by extrusion method for liposome preparation, in: Methods Mol. Biol. 1522, Humana Press Inc., 2017, pp. 17–22, https://doi.org/10.1007/978-1-4939-6591-5_2.

[27] R. Fudala, M.E. Mummert, Z. Gryczynski, R. Rich, J. Borejdo, I. Gryczynski, Lifetime-based sensing of the hyaluronidase using fluorescein labeled hyaluronic acid, J. Photochem. Photobiol. B Biol. 106 (2012) 69–73, https://doi.org/10.1016/j.jphotobiol.2011.10.005.

[28] T. Parasassi, E.K. Krasnowska, L. Bagatolli, E. Gratton, Laurdan and Prodan as polarity-sensitive fluorescent membrane probes, J. Fluoresc. 8 (1998) 365–373, https://doi.org/10.1023/A:1020528716621.

[29] H. Zhang, S.C. De Smedt, K. Remaut, Fluorescence correlation spectroscopy to find the critical balance between extracellular association and intracellular dissociation of mRNA complexes, Acta Biomater. 75 (2018) 358–370, https://doi.org/10.1016/j.actbio.2018.05.016.

[30] A. Okazaki, J.-I. Jo, Y. Tabata, A reverse transfection technology to genetically engineer adult stem cells, Tissue Eng. 13 (2007) 245–251, https://doi.org/10.1089/ten.2006.0185.

[31] H. Tanaka, T. Takahashi, M. Konishi, N. Takata, M. Gomi, D. Shirane, et al., Self-degradable lipid-like materials based on “hydrolysis accelerated by the intra-particle enrichment of reactant (HyPER)” for messenger RNA delivery, Adv. Funct. Mater. 30 (2020) 1910575, https://doi.org/10.1002/adfm.201910575.

[32] L.M. Kranz, M. Diken, H. Haas, S. Kreiter, C. Loquai, K.C. Reuter, et al., Systemic RNA delivery to dendritic cells exploits antiviral defence for cancer immunotherapy, Nature 534 (2016) 396–401, https://doi.org/10.1038/nature18300.

[33] Q. Cheng, T. Wei, L. Farbiak, L.T. Johnson, S.A. Dilliard, D.J. Siegwart, Selective organ targeting (SORT) nanoparticles for tissue-specific mRNA delivery and CRISPR–Cas gene editing, Nat. Nanotechnol. 15 (2020) 313–320, https://doi.org/10.1038/s41565-020-0669-6.

[34] S. Rosigkeit, M. Meng, C. Grunwitz, P. Gomes, A. Kreft, N. Hayduk, et al., Monitoring translation activity of mRNA-loaded nanoparticles in mice, Mol. Pharm. 15 (2018) 3909–3919, https://doi.org/10.1021/acs.molpharmaceut.8b00370.

[35] A.A.M. Gasperini, X.E. Puentes-Martinez, T.A. Balbino, Rigoletto T. De Paula, G. De Sá Cavalcanti Corrêa, A. Cassago, et al., Association between cationic liposomes and low molecular weight hyaluronic acid, Langmuir 31 (2015) 3308–3317, https://doi.org/10.1021/la5045865.

[36] S.A. Sanchez, M.A. Tricerri, G. Gunther, E. Gratton, Laurdan generalized polarization: from cuvette to microscope, Mod. Res. Educ. Top. Microsc. 2 (2007) 1007–1014.

[37] Y. Weng, C. Li, T. Yang, B. Hu, M. Zhang, S. Guo, et al., The challenge and prospect of mRNA therapeutics landscape, Biotechnol. Adv. (2020) 40, https://doi.org/10.1016/j.biotechadv.2020.107534.

[38] J. Bompard, A. Rosso, L. Brizuela, S. Mebarek, L.J. Blum, A.M. Trunfio-Sfarghiu, et al., Membrane fluidity as a new means to selectively target cancer cells with fusogenic lipid carriers, Langmuir 36 (2020) 5134–5144, https://doi.org/10.1021/acs.langmuir.0c00262.

[39] W. Li, F.C. Szoka, Lipid-based nanoparticles for nucleic acid delivery, Pharm. Res. 24 (2007) 438–449, https://doi.org/10.1007/s11095-006-9180-5.

[40] A. Ziller, S.S. Nogueira, E. Hühn, S.S. Funari, G. Brezesinski, H. Hartmann, et al., Incorporation of mRNA in lamellar lipid matrices for parenteral administration, Mol. Pharm. 15 (2018) 642–651, https://doi.org/10.1021/acs.molpharmaceut.7b01022.

[41] S. Weisman, D. Hirsch-Lerner, Y. Barenholz, Y. Talmon, Nanostructure of cationic lipid-oligonucleotide complexes, Biophys. J. 87 (2004) 609–614, https://doi.org/10.1529/biophysj.103.033480.

[42] D. Peer, J. Lieberman, Special delivery: targeted therapy with small RNAs, Gene Ther. 18 (2011) 1127–1133, https://doi.org/10.1038/gt.2011.56.

[43] C.D. Siewert, H. Haas, V. Cornet, S.S. Nogueira, T. Nawroth, L. Uebbing, et al., Hybrid biopolymer and lipid nanoparticles with improved transfection efficacy for mRNA, Cells (2020) 9, https://doi.org/10.3390/cells9092034.

[44] C. Wang, X. Li, S.D. Wettig, I. Badea, M. Foldvari, R.E. Verrall, Investigation of complexes formed by interaction of cationic gemini surfactants with deoxyribonucleic acid, Phys. Chem. Chem. Phys. 9 (2007) 1616–1628, https://doi.org/10.1039/b618579g.

[45] T.K. Dam, M.L. Talaga, N. Fan, C.F. Brewer, Measuring multivalent binding interactions by isothermal titration calorimetry, Methods Enzymol. 567 (2016) 71–95, https://doi.org/10.1016/bs.mie.2015.08.013.

[46] I. Koltover, T. Salditt, C.R. Safinya, Phase diagram, stability, and overcharging of lamellar cationic lipid- DNA self-assembled complexes, Biophys. J. 77 (1999) 915–924, https://doi.org/10.1016/S0006-3495(99)76942-0.

[47] E. Pozharski, R.C. MacDonald, Thermodynamics of cationic lipid-DNA complex formation as studied by isothermal titration calorimetry, Biophys. J. 83 (2002) 556–565, https://doi.org/10.1016/S0006-3495(02)75191-6.

[48] K. Buyens, B. Lucas, K. Raemdonck, K. Braeckmans, J. Vercammen, J. Hendrix, et al., A fast and sensitive method for measuring the integrity of siRNA-carrier complexes in full human serum, J. Control. Release 126 (2008) 67–76, https://doi.org/10.1016/j.jconrel.2007.10.024.

[49] H. Zhang, K. Rombouts, L. Raes, R. Xiong, S.C. De Smedt, K. Braeckmans, et al., Fluorescence-based quantification of messenger RNA and plasmid DNA decay kinetics in extracellular biological fluids and cell extracts, Adv. Biosyst. 4 (2020) 2000057, https://doi.org/10.1002/adbi.202000057.

[50] H. Bosshart, M. Heinzelmann, THP-1 cells as a model for human monocytes, Ann. Transl. Med. (2016) 4, https://doi.org/10.21037/atm.2016.08.53.

[51] A. Rosso, V. Andretto, Y. Chevalier, D. Kryza, J. Sidi-Boumedine, A. Grenha, et al., Nanocomposite sponges for enhancing intestinal residence time following oral administration, J. Control. Release 333 (2021) 579–592, https://doi.org/10.1016/j.jconrel.2021.04.004.

[52] R.A. Meyer, G.P. Hussmann, N.C. Peterson, J.L. Santos, A.D. Tuesca, A scalable and robust cationic lipid/polymer hybrid nanoparticle platform for mRNA delivery, Int. J. Pharm. 611 (2022), 121314, https://doi.org/10.1016/j.ijpharm.2021.121314.

[53] L. Cassetta, J.W. Pollard, Targeting macrophages: therapeutic approaches in cancer, Nat. Rev. Drug Discov. 17 (2018) 887–904, https://doi.org/10.1038/nrd.2018.169.

[54] S. Watanabe, M. Alexander, A.V. Misharin, G.R.S. Budinger, The role of macrophages in the resolution of inflammation, J. Clin. Invest. 129 (2019) 2619–2628, https://doi.org/10.1172/JCI124615.